Anal. Bioanal. Electrochem., Vol. 16, No. 10, 2024, 967-977
https://www.doi.org/10.22034/abec.2024.717553

Analytical & Bioanalytical Electrochemistry

Full Paper

NS-RGO-Cu-MOF Composite: An Efficient Electrocatalyst for Dual Hydrogen and Oxygen Evolution Reactions

Seyed Ali Mousavi,[1,2,3] Mehdi Mehrpooya[2,3,*]

[1]*School of Mechanical Engineering, Shiraz University, Shiraz, Iran*
[2]*School of Energy Engineering and Sustainable Resources, College of Interdisciplinary Science and Technology, University of Tehran, Tehran, Iran*
[3]*Hydrogen and Fuel Cell Laboratory, University of Tehran, Tehran, Iran*

*Corresponding Author,
E-Mail: mehrpoya@ut.ac.ir

Received: 11 August 2024 / Received in revised form: 19 October 2024 / Accepted: 25 October 2024 / Published online: 31 October 2024

Abstract- In this experimental study, a highly efficient NS-RGO–Cu-MOF electrocatalyst was developed for electrochemical water splitting, encompassing both the Hydrogen Evolution Reaction (HER) and Oxygen Evolution Reaction (OER). First, nitrogen- and sulfur-doped reduced graphene oxide (NS-RGO) was synthesized by fabricating GO via Hummer's method, followed by a condensation technique at 190°C. Next, a copper-centered metal-organic framework (Cu-MOF) electrocatalyst was produced using a solvothermal approach. Finally, the Cu-MOF was loaded onto the NS-RGO substrate at a specified weight percentage via pyrolysis at 750°C under nitrogen flow. The synthesized composite was characterized using six analytical techniques, confirming its desirable morphology. The electrochemical water-splitting performance was evaluated using a three-electrode configuration under standard conditions, yielding onset potential values of 0.65 V vs. Ag/AgCl and -0.98 V vs. Ag/AgCl for OER and HER, respectively. Due to the synergistic effects between the NS-RGO substrate and the Cu-MOF composite, the electrocatalyst exhibited significantly enhanced electrical conductivity, stability, and catalytic activity, showing promise as an alternative to Pt-based electrocatalysts for electrochemical water-splitting applications.

Keywords- Hydrogen Evolution Reaction; Oxygen Evolution Reaction; Electrocatalysis; Metal Organic Framework

1. INTRODUCTION

Electrochemical water splitting is a promising technology for sustainable hydrogen production, a clean energy carrier that can mitigate the challenges posed by fossil fuel dependence and greenhouse gas emissions [1]. The process involves two key electrochemical reactions: the hydrogen evolution reaction (HER) and the oxygen evolution reaction (OER) [2]. HER typically occurs at the cathode, where protons are reduced to produce hydrogen gas, while OER takes place at the anode, where water molecules are oxidized to release oxygen gas [3].

Traditionally, platinum (Pt) has been the benchmark electrocatalyst for HER due to its excellent activity, stability, and low overpotential requirements. Similarly, noble metal oxides such as iridium (Ir) and ruthenium (Ru) are favored for OER owing to their high catalytic efficiency. However, the scarcity, high cost, and limited availability of these precious metals pose significant challenges for the large-scale deployment of water splitting technologies [4].

To overcome these limitations, there is a growing necessity for non-Pt electrocatalysts that can provide comparable or enhanced performance at a lower cost and with improved sustainability. Non-noble metal-based materials, including transition metal dichalcogenides (TMDs), metal-organic frameworks (MOFs), and conducting polymers, have emerged as promising alternatives. These materials often exhibit unique catalytic properties and can be engineered to optimize their performance for HER and OER, thus paving the way for more accessible and economically viable hydrogen production.

In this context, understanding the mechanisms of HER and OER is crucial. The HER involves the reduction of protons (H^+) to form hydrogen gas (H_2) through either the Volmer step (proton adsorption), followed by the Heyrovsky step (recombination with another proton), or the Tafel step (recombination with an adsorbed hydrogen atom). On the other hand, OER is characterized by the oxidation of water molecules, which involves multiple electron transfer steps leading to the formation of oxygen gas (O_2) [5].

In the past year, significant advancements have been made in the development of non-Pt electrocatalysts. Researchers have focused on transition metal catalysts, such as nickel, cobalt, and iron-based materials, which have shown impressive electrocatalytic activity [6]. The integration of these metals with conductive materials has led to improved efficiency and stability. Additionally, new strategies involving the design of hybrid systems that combine different active components have emerged, leading to catalysts that perform well for both HER and OER [7]. Innovations in material synthesis, such as controlling morphology and introducing defects, have further enhanced catalytic performance. These developments indicate a robust trend toward finding effective non-Pt alternatives that can meet the efficiency and cost requirements for practical electrochemical water splitting.

Using non-Pt electrocatalysts for HER and OER is crucial to improve the cost, availability, and durability of water-splitting technologies.

The NS-RGO–Cu-MOF electrocatalyst has been synthesized by the current team for application in the Oxygen Reduction Reaction (ORR) [8]. In this research, this composite is used for electrochemical water splitting applications. The HER and OER performance are investigated using the onset potential values. Loading Cu-MOF onto NS-RGO substrates significantly enhances performance for HER and OER applications. This improvement is primarily due to the high electrical conductivity of NS-RGO, which facilitates better electron transport, and the high surface area of Cu-MOFs that increases exposure to active sites, thereby boosting catalytic activity. The porous structure of Cu-MOFs enhances mass transport, allowing reactants to access active sites more efficiently. Additionally, the synergistic effects between Cu-MOF and NS-RGO optimize the electronic properties of the catalyst, improving the adsorption energies of reaction intermediates and lowering the overpotentials required for both HER and OER.

2. METHODOLOGY

This section provides an overview of the synthesis protocol employed, the characterization techniques utilized, and the operating conditions for the electrochemical examinations.

2.1. Synthesis of 8% NS-RGO – Cu-MOF electrocatalyst

The procedure for synthesizing the 8% NS-RGO–Cu-MOF electrocatalyst, including detailed steps, has been provided in our previous study [8]. In brief, thiourea was used as a reductant to reduce graphene oxide (GO) and dope it with nitrogen and sulfur [9]. GO (50 mg) was dispersed in ethylene glycol (EG) using an ultrasonic bath, followed by adding a thiourea solution prepared separately. The solution was sonicated for 90 minutes, then refluxed at 190°C for 5 hours. The resulting NS-RGO was isolated by centrifugation, washed, and dried in a vacuum oven, yielding a black powder indicating successful doping [10].

To synthesize the Cu-MOF composite, Copper nitrate trihydrate was mixed with 1,4-benzenedicarboxylic acid and triethylenediamine in dimethylformamide (DMF). Then, the mixture was sonicated for 1 hour and heated in an autoclave at 120°C for 36 hours. After cooling and washing, the turquoise-blue Cu-MOF powder was obtained by drying in a vacuum oven [11]. Finally, 8 wt% NS-RGO was incorporated into the Cu-MOF and sonicated for 2 hours. The mixture was heated again in an autoclave at 120°C for 36 hours, then washed and dried. To enhance conductivity, the 8% NS-RGO–Cu-MOF was pyrolyzed at 750°C in an N_2 atmosphere, resulting in a blue-gray powder.

2.2. Materials Characterization

In this study, a range of physical characterization techniques was employed to analyze the synthesized materials. X-ray diffraction (XRD) was used to assess the crystalline structure,

providing information on phase purity and particle size [12]. Scanning Electron Microscopy (SEM) examined surface morphology, while Transmission Electron Microscopy (TEM) offered detailed insights into internal microstructures [13]. Elemental composition was determined using Energy-Dispersive X-ray Spectroscopy (EDS), and Fourier Transform Infrared (FTIR) spectroscopy was conducted to identify functional groups and chemical bonds. The model of each instrument and the operational conditions used for these analyses are provided in the references [8,14].

2.3. Electrochemical behavior analysis

The technical performance of the synthesized electrocatalyst for electrochemical water splitting application was investigated using standard Rotary Disc Electrode (RDE) setup. A glassy carbon electrode (GCE) with a 2 mm diameter served as the base for the working electrode. Before use, the working electrode was mechanically polished using an alumina slurry to achieve a mirror finish, then rinsed with deionized (DI) water and acetone, and allowed to air dry. Then, a suspension was prepared by dispersing 2 mg of the NS-RGO – Cu-MOF powder with 20 µL of a 5 wt.% Nafion solution in a 1:1 mixture of ethanol and deionized water, then sonicating for 45 minutes to form an ink. Next, 10 µL of this ink was applied to the GCE surface and dried under IR light at room temperature. The reference electrode used was an Ag/AgCl electrode in saturated KCl, while a platinum wire functioned as the counter electrode [15]. To assess the electrocatalytic activity and obtain the onset potential value, Linear Sweep Voltammetry (LSV) was conducted at a scan rate of 10 $mV \cdot s^{-1}$ and a rotation speed of 1500 rpm. The HER behavior was evaluated in a nitrogen-saturated 0.5 M H_2SO_4 solution, while the OER performance was tested in an oxygen-saturated 1 M KOH solution [16]. Additionally, the stability of the prepared sample was examined using a chronoamperometry test at -0.4 V vs. Ag/AgCl over a duration of 2000 s.

The synthesis procedure, along with the evaluation methodologies for the produced electrocatalyst, is presented at a glance in Figure 1.

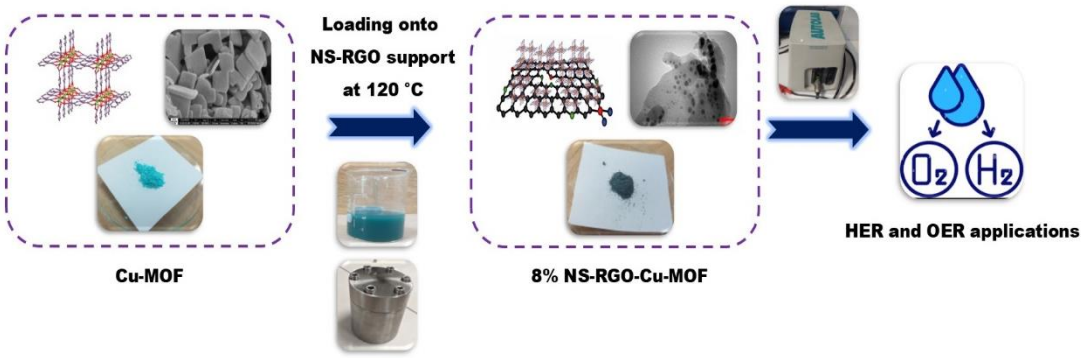

Figure 1. Overview of the synthesis procedure and evaluation methodologies for the 8%NS-RGO – Cu-MOF electrocatalyst

3. RESULTS AND DISCUSSION

The characterization examinations and the results of the electrochemical behavior analysis of the prepared samples are presented in this section.

Figure 2 indicates the XRD patterns of the developed electrocatalysts. The XRD pattern of NS-doped RGO shows that the GO peak at (001) vanishes after thiourea reduction. A new peak emerges at 2θ = 25° (002), with a d-spacing of 0.4 nm, indicating that nitrogen and sulfur atoms have likely substituted the oxygen functional groups [17]. "As evident in the XRD analysis, the two main peaks of the MOF structure, corresponding to (101) and (211), are observed. New peaks have appeared due to the loading of MOF on the NS-RGO surface. Additionally, a reduction in peak intensity can be seen, which results from decreased crystallinity caused by the incorporation of MOFs between the layers of NS-RGO. The peak associated with NS-RGO appears with very low intensity, likely due to the loading of MOFs on the graphene sheets [18]. It is also evident that a significant number of peaks have disappeared. After the pyrolysis process, the crystalline structure of the MOF has broken down, with some ligands being removed. The peaks at (111) and (022) correspond to pure copper [19]. The observed peaks confirm that the MOF structure has been successfully loaded onto the NS-RGO surface. The reduction in peak intensity and the disappearance of some peaks indicate a loss of crystallinity in the MOF due to the pyrolysis process and the presence of graphene layers. Additionally, the formation of pure copper supports this structural change.

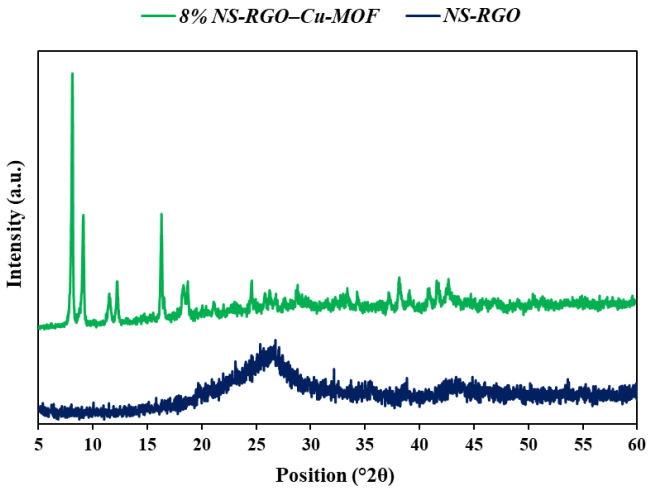

Figure 2. The XRD patterns of the fabricated samples

The FTIR analysis results for each sample are presented in Figure 3. In the FTIR spectrum of NS-RGO, it is observed that the peak width associated with the hydroxyl group (O-H) is reduced compared to GO. Additionally, due to the removal of oxygen functional groups, the intensity of the peak related to the carbonyl group (C=O) is significantly decreased [20]. Furthermore, a new peak appears at 1206 cm^{-1}, corresponding to the stretching vibration of the

C-N group. These results indicate that the reduction of GO has been successfully achieved. In the FTIR spectrum of Cu-MOF, the broad peak at 3434.04 cm^{-1} corresponds to the O-H stretching vibration. The peak at 2931 cm^{-1} is attributed to the symmetric stretching vibration of O-H [21]. The peak at 1675.51 cm^{-1} is related to the C=O vibration from the COOH group. The peak at 472.71 cm^{-1} is also associated with copper-N. Using NS-RGO instead of GO reduces the intensity of the oxygen functional groups. Additionally, the intensity of the hydroxyl (O-H) group at 3434.04 cm^{-1} is reduced compared to GO-Cu-MOF. The peak at 1593 cm^{-1} corresponds to C=C and C=N bands [22]. The main peaks associated with Cu-MOF, GO, and NS-RGO are also observed in the FTIR spectrum for NS-RGO-Cu-MOF. The FTIR results indicate that the reduction of GO to NS-RGO was successfully achieved, leading to a decrease in oxygen functional groups and enhancing the conductive structure in the electrocatalysts. This modification effectively supports the formation of Cu-MOF crystals on NS-RGO sheets.

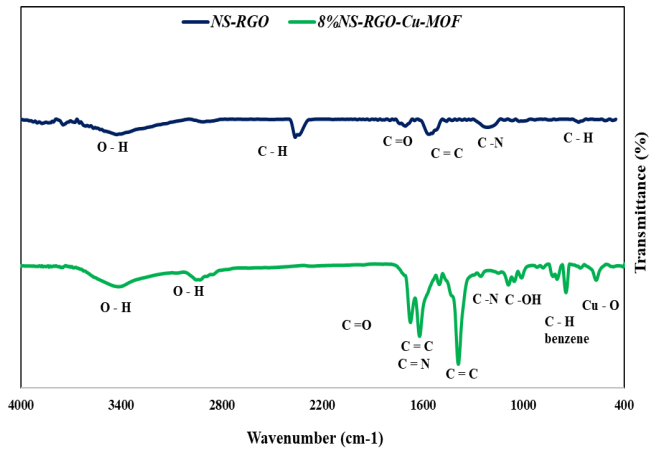

Figure 3. The FTIR spectral profiles for each sample

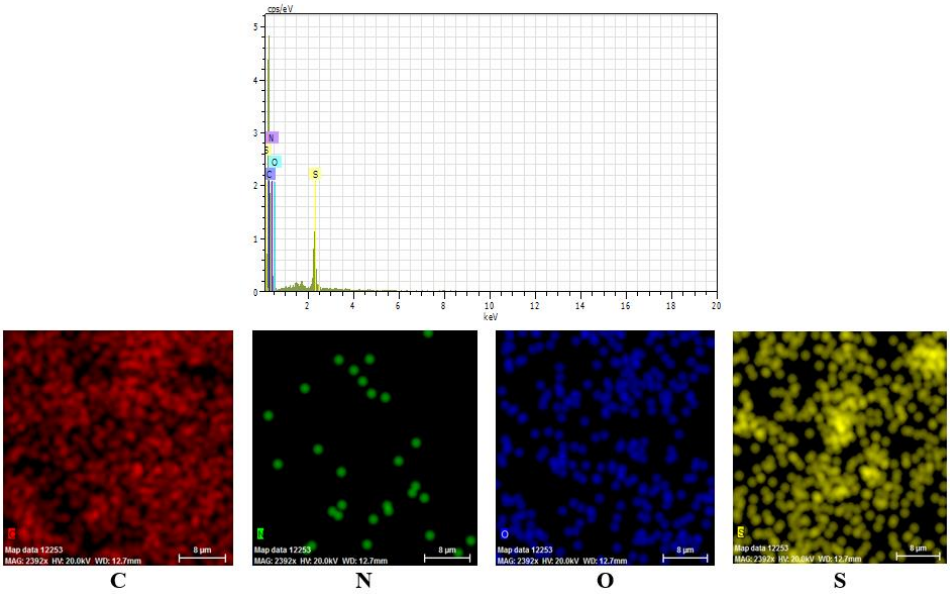

Figure 4. EDS and elemental mapping analyses of the NS-RGO substrate

After the reduction of GO using a thiourea reductant, the elemental composition and distribution were investigated through EDS and elemental mapping techniques (Figure 4). The results confirm that all elements are uniformly and successfully incorporated throughout the structure, indicating effective reduction and doping.

Figure 5 illustrates the SEM images of the prepared samples. The SEM image of the Cu-MOF sample (A) reveals a highly crystalline, angular morphology, typical of metal-organic frameworks. The uniformity and well-defined edges of these crystals suggest successful synthesis of Cu-MOF with a consistent structure, which is beneficial for providing numerous active sites for catalytic applications [11]. In the SEM image of NS-RGO (B), the structure appears less crystalline and more layered, indicative of reduced graphene oxide (RGO). The sheet-like morphology, combined with visible roughness, is consistent with nitrogen and sulfur doping, which may introduce additional defects and enhance surface area, aiding in catalytic performance [23].

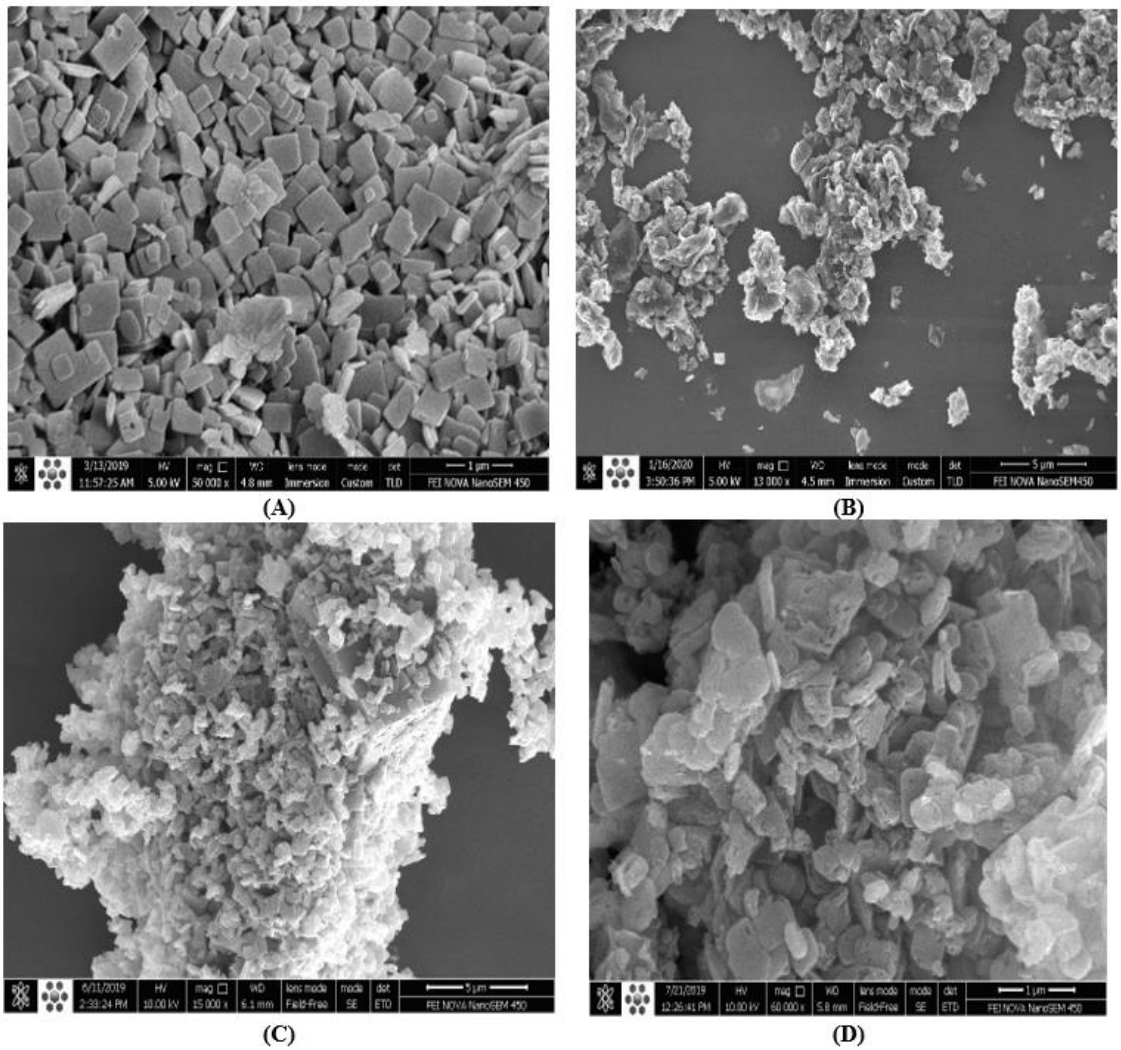

Figure 5. The SEM images of the prepared samples: (A) Cu-MOF; (B) NS-RGO; (C-D) 8% NS-RGO–Cu-MOF

Removing oxygen functional groups does indeed bring the sheets closer together, but it's primarily due to the reduction in interlayer spacing and the reformation of π-π interactions between graphene layers [24]. The SEM images of the 8% NS-RGO–Cu-MOF composite (C-D) display a combination of Cu-MOF particles distributed on the NS-RGO sheets. The images suggest good dispersion of Cu-MOF on the graphene surface, without significant aggregation. This distribution is essential for maximizing the interfacial area between Cu-MOF and NS-RGO, facilitating electron transfer and improving catalytic activity. The presence of Cu-MOF particles across the graphene support indicates successful loading, which contributes to the stability and electrical conductivity of the composite, benefiting HER and OER reactions.

The TEM images of the 8% NS-RGO–Cu-MOF composite with a resolution of 50 nm are presented in Figure 6. The TEM images provide a closer look at the nanoscale structure of the 8% NS-RGO–Cu-MOF composite. Cu-MOF nanoparticles appear as darker spots, well-dispersed on the NS-RGO sheets. This dispersion at the nanoscale confirms effective integration, indicating that the solvothermal synthesis method enabled fine control over particle size and placement. The spacing and distribution of particles on NS-RGO further ensure optimal exposure of active sites and contribute to enhanced catalytic performance by maintaining a conductive pathway for electron transfer during electrochemical reactions [22].

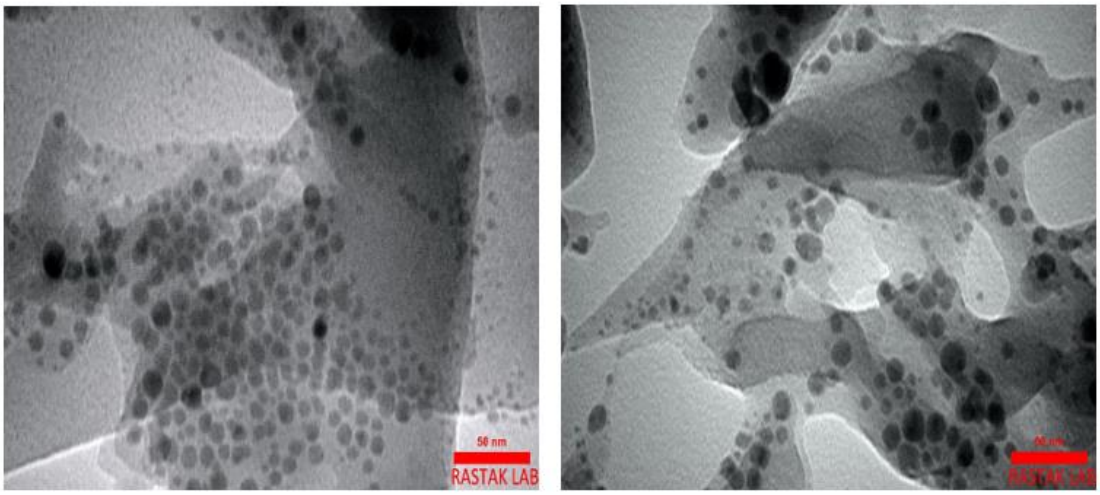

Figure 6. The TEM images of the 8% NS-RGO–Cu-MOF electro-catalyst

Figure 7 illustrates the electrochemical behavior of the fabricated samples in HER and OER. In evaluating the electrochemical performance for the HER and OER at 1500 rpm, distinct improvements are observed when Cu-MOF is loaded onto NS-RGO compared to Cu-MOF alone. For HER, the onset potential of the Cu-MOF electrode is around -1.1 V vs. Ag/AgCl, while the NS-RGO-Cu-MOF composite exhibits a more favorable onset potential of approximately -0.98 V vs. Ag/AgCl, indicating that the NS-RGO-Cu-MOF initiates hydrogen evolution at a lower voltage. The maximum current density achieved by NS-RGO-Cu-MOF is

around -60 mA/cm², compared to -30 mA/cm² for Cu-MOF alone, suggesting a more efficient electron transfer process facilitated by the NS-RGO support. This improvement is due to the high conductivity and surface area of NS-RGO, which enhances electron mobility and provides more active sites for HER. The voltage range for HER spans from approximately -1.4 V to 0 V vs. Ag/AgCl.

In the case of OER, NS-RGO-Cu-MOF again demonstrates superior performance with an onset potential of approximately 0.65 V vs. Ag/AgCl, compared to 0.8 V vs. Ag/AgCl for Cu-MOF alone. The maximum current density for NS-RGO-Cu-MOF reaches around 16 mA/cm², while Cu-MOF alone achieves about 6 mA/cm². The enhanced current density for NS-RGO-Cu-MOF in the positive voltage range (up to 1 V vs. Ag/AgCl) suggests that NS-RGO effectively lowers the energy barrier for oxygen evolution, likely by improving conductivity and facilitating a faster charge transfer process. The voltage range for OER spans from -0.4 V to 1 V vs. Ag/AgCl.

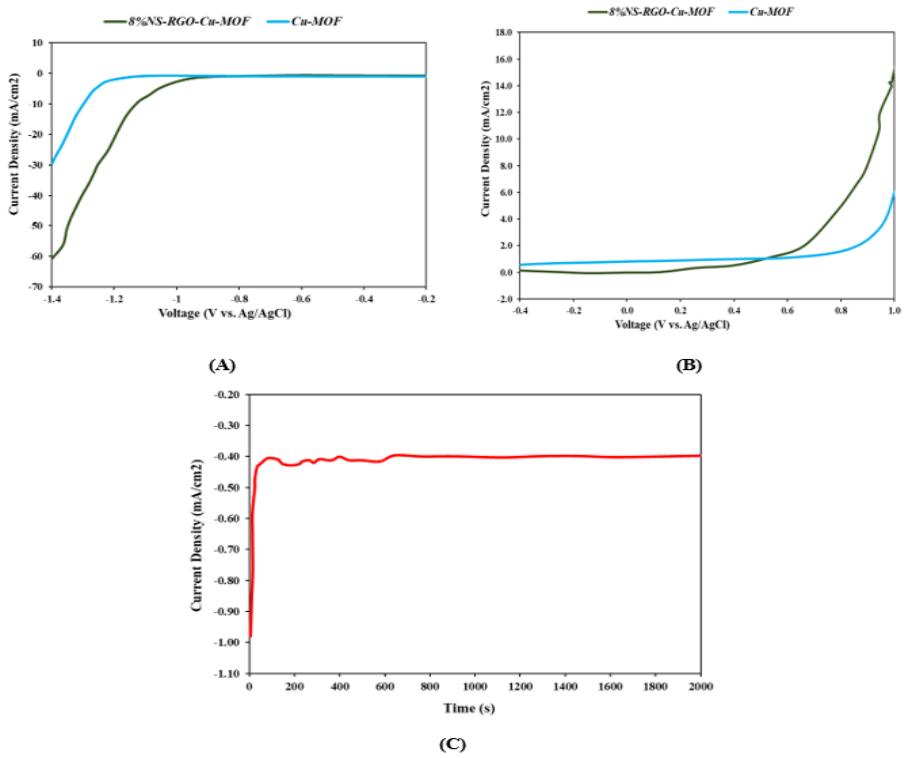

Figure 7. The electrochemical behavior for electrochemical water splitting using the fabricated electrocatalyst: (A) HER; (B) OER; (C) chronoamperometry test of the NS-RGO-Cu-MOF catalyst in 1 M KOH

The chronoamperometry test of the NS-RGO-Cu-MOF catalyst in 1 M KOH over 2000 seconds demonstrates stable performance, likely due to the composite's robust structure, where NS-RGO enhances the mechanical integrity and prevents Cu-MOF particles from agglomerating or detaching. Additionally, NS-RGO provides corrosion resistance in the

alkaline environment and ensures high conductivity, facilitating efficient electron transport and reducing surface resistive layers. These factors contribute to the catalyst's durability and sustained activity under prolonged electrochemical conditions.

Loading Cu-MOF onto NS-RGO significantly improves the electrocatalytic performance in both HER and OER. This enhancement can be attributed to NS-RGO's conductive and structural properties, which aid in reducing the onset potential and increasing the maximum current density, thereby promoting efficient electrocatalytic activity for both reactions.

4. CONCLUSION

This empirical investigation aims to introduce an efficient electrocatalyst for electrochemical water splitting. To this end, an 8% NS-RGO–Cu-MOF electrocatalyst was prepared by loading Cu-MOF onto an NS-RGO substrate using a solvothermal method at 120°C, followed by pyrolysis in an N_2 atmosphere at 750°C. The successful loading of Cu-MOF particles onto the carbon-based support, as well as the desirable morphology, were confirmed through characterization techniques. Based on electrochemical examinations, the onset potential for HER and OER was found to be -0.98 V vs. Ag/AgCl and 0.65 V vs. Ag/AgCl, respectively, indicating that the synergistic effect between the porous structure of Cu-MOFs and the high electrical conductivity of the NS-RGO support can significantly improve the water-splitting process. The total active site density is increased, allowing more sites to participate in electrochemical reactions. NS-RGO acts as a highly conductive and stable support, ensuring these active sites are both well-dispersed and structurally supported, thereby enhancing overall catalytic activity. Cu atoms within the MOF provide HER-active sites, while N and S dopants in the RGO influence the electronic structure, increasing electron density around Cu sites and optimizing their binding with reaction intermediates.

Acknowledgments

This work has been supported by the Center for International Scientific Studies & Collaborations (CISSC) Ministry of Science Research and Technology of Iran.

Declarations of interest

The authors declare no conflict of interest in this reported work.

REFERENCES

[1] M. Mehrpooya, B. Ghorbani, A. Ekrataleshian, and S.A. Mousavi, Int. J. Energy Res. 45 (2021) 14845.

[2] D.D. Qin, Y. Tang, G. Ma, L. Qin, C.L. Tao, X. Zhang, and Z. Tang, Int. J. Hydrogen Energy 46 (2021) 25771.

[3] T. Wang, P. Wang, W. Zang, X. Li, D. Chen, Z. Kou, S. Mu, and J. Wang, Advanced Functional Materials 32 (2022) 2107382.
[4] M. Zubair, M.M.U. Hassan, M.T. Mehran, M.M. Baig, S. Hussain, and F. Shahzad, Int. J. Hydrogen Energy 47 (2022) 2794.
[5] A. Alobaid, C. Wang, and R.A. Adomaitis, J. Electrochem. Soc. 165 (2018) J3395.
[6] M.R. Kandel, U.N. Pan, D.R. Paudel, P.P. Dhakal, N.H. Kim, and J.H. Lee, Composites B: Engineering 239 (2022) 109992.
[7] R. Zahra, E. Pervaiz, M. Yang, O. Rabi, Z. Saleem, M. Ali, and S. Farrukh, Int. J. Hydrogen Energy 45 (2020) 24518.
[8] S.A. Mousavi, and M. Mehrpooya, Energy 214 (2021) 119053.
[9] S. Pei, and H.M. Cheng, Nanoscale 5 (2013) 1753.
[10] M. Jahan, Z. Liu, and K.P. Loh, Advanced Functional Materials 23 (2013) 5363.
[11] S.A. Mousavi, M. Mehrpooya, and M.R. Ganjali, Int. J. Hydrogen Energy 51 (2024) 787.
[12] M. Mehrpooya, F. Valizadeh, R. Askarimoghadam, S. Sadeghi, F. Pourfayaz, and S.A. Mousavi, The European Physical Journal Plus 135 (2020) 1.
[13] S.A. Mousavi, M. Mehrpooya, and M.R. Ganjali, Materials Chemistry and Physics 320 (2024) 129394.
[14] H. Kamali, M. Mehrpooya, S.A. Mousavi, and M.R. Ganjali, New Journal of Chem. 46 (2022) 18351.
[15] Y. Pan, K. Sun, S. Liu, X. Cao, K. Wu, W.C. Cheong, Z. Chen, Y. Wang, Y. Li, and Y. Liu, J. American Chem. Soc. 140 (2018) 2610.
[16] S.A. Soomro, I.H. Gul, H. Naseer, S. Marwat, and M. Mujahid, Current Nanoscience 15 (2019) 420.
[17] G. Liu, Y. Zhou, C. Zou, X. Zhu, and Y. Guo, J. Mater. Sci.: Mater. Electron. 29 (2018) 3317.
[18] D.N. Dybtsev, H. Chun, and K. Kim, Angewandte Chemie International Edition 43 (2004) 5033.
[19] B.P. Vinayan, 177 (2016).
[20] J.M. You, M.S. Ahmed, H.S. Han, J. eun Choe, Z. Üstündağ, and S. Jeon, Journal of Power Sources 275 (2015) 73.
[21] K. Yang, Y. Yan, H. Wang, Z. Sun, W. Chen, H. Kang, Y. Han, W. Zahng, X. Sun, and Z. Li, Nanoscale 10 (2018) 17647.
[22] S. Bag, B. Mondal, A.K. Das, and C.R. Raj, Electrochim. Acta 163 (2015) 16.
[23] L.M. Rivera, S. Fajardo, M.d.C. Arévalo, G. García, and E. Pastor, Catalysts 7 (2017) 278.